



AUTHOR(S):

TITLE:

YEAR:

Publisher citation:

OpenAIR citation:

Publisher copyright statement:

This is the _____ version of an article originally published by _____
in _____
(ISSN _____; eISSN _____).

OpenAIR takedown statement:

Section 6 of the "Repository policy for OpenAIR @ RGU" (available from <http://www.rgu.ac.uk/staff-and-current-students/library/library-policies/repository-policies>) provides guidance on the criteria under which RGU will consider withdrawing material from OpenAIR. If you believe that this item is subject to any of these criteria, or for any other reason should not be held on OpenAIR, then please contact openair-help@rgu.ac.uk with the details of the item and the nature of your complaint.

This publication is distributed under a CC _____ license.

1 **A novel endurance prediction method of series connected lithium-ion batteries based on the**
2 **voltage change rate and iterative calculation**

3 **Shun-Li Wang^{a*}, Wu Tang^b, Carlos Fernandez^c, Chun-Mei Yu^a, Xiao-Xia Li^a, Xiao-Qin Zhang^a**

4 *^aSchool of Information Engineering, Southwest University of Science and Technology, Mianyang 621010,*
5 *China; ^b School of Materials and Energy, University of Electronic Science and Technology of China, 611731,*
6 *Chengdu, China; ^cSchool of Pharmacy and Life Sciences, Robert Gordon University, Aberdeen AB10-7GJ, UK.*

7

8 **Abstract:** High-power lithium-ion battery packs are widely used in large and medium-sized unmanned aerial vehicles
9 and other fields, but there is a safety hazard problem with the application that needs to be solved. The generation
10 mechanism and prevention measurement research is carried out on the battery management system for the unmanned aerial
11 vehicles and the lithium-ion battery state monitoring. According to the group equivalent modeling demand against the
12 battery packs, a new idea of compound equivalent circuit modeling is proposed and the model constructed to realize the
13 accurate description of the working characteristics. In order to realize the high-precision state prediction, the improved
14 unscented Kalman feedback correction mechanism is introduced, in which the simplified particle transformation is
15 introduced and the voltage change rate is calculated to construct a new endurance prediction model. Aiming at the
16 influence of the consistency difference between battery cells, a novel equilibrium state evaluation idea is applied and the
17 calculation results are embedded in the equivalent modeling and iterative calculation to improve the prediction accuracy.
18 The model parameters are identified by the Hybrid Pulse Power Characteristic test, in which the conclusion is that the mean
19 value of the ohm internal resistance is 20.68mΩ. The average internal resistance is 1.36mΩ, and the mean capacitance
20 value is 47747.9F. The state of charge prediction error is less than 2%, which provides a feasible way for the equivalent
21 modeling, battery management system design and practical application of pack working lithium-ion batteries.

22 **Key words:** Lithium-ion battery; endurance prediction; equivalent model; voltage change rate; unmanned aerial vehicles

23 ***Corresponding author:** Shun-Li Wang. Tel: +86-15884655563. E-mail address: wangshunli@swust.edu.cn.

24 1. Introduction

25 Large and medium-sized Unmanned Aerial Vehicles (UAV) refers to a battery that is fully charged beforehand and
26 supplied to the electric motor. At the same time, the battery is supplemented by an external power source, which has the
27 advantages of low pollution, low noise, high energy efficiency and diversified energy sources. Because they are suitable for
28 the UAV application, lithium-ion batteries are widely used due to low price and excellent cycle performance advantages, as
29 well as having broad prospects of the power supply field.

30 The Battery-Management-System (BMS) construction method was conducted for the real-time working state monitoring
31 and energy management of the lithium-ion battery packs. Vortex generators were constructed for the active thermal
32 management in lithium-ion battery power supply systems (Mondal, Lopez, Verma, & Mukherjee, 2018). Comparative
33 analysis of lithium-ion battery resistance prediction was realized for the BMS (Mathew, Janhunen, Rashid, Long, &
34 Fowler, 2018). Water cool strategy was studied for the thermal management system of the lithium-ion battery pack (Li,
35 Yan, Chen, & Wang, 2018). Experimental investigation of the thermal management system was conducted for lithium-ion
36 battery modules with coupling effect by heat sheets and phase change materials (He, Li, Zhang, Zhong, & He, 2018).
37 Issues and recommendations were analyzed for the energy management system of lithium-ion batteries (Hannan, Hoque,
38 Hussain, Yusof, & Ker, 2018). Impedance-based BMS was designed for the safety monitoring of lithium-ion batteries
39 (Carkhuff, Demirev, & Srinivasan, 2018). Thermal management system of lithium-ion battery module was realized by
40 using the micro heat pipe array (X. Ye, Zhao, & Quan, 2018). Lifetime management method was investigated for the
41 energy storage system of lithium-ion batteries (Won, Choo, Lee, Lee, & Won, 2018). Performance analysis of the thermal
42 management system was conducted with composite phase change material for lithium-ion battery packs (X. M. Wang et
43 al., 2018). A novel thermal management system was constructed by using the mist cooling method of lithium-ion battery
44 packs (Saw et al., 2018). Afterwards, health management systems were reviewed for lithium-ion batteries (Omariba,
45 Zhang, & Sun, 2018).

46 The Equivalent-Circuit-Modeling (ECM) analysis was conducted by mounts of researchers. The State of Charge (SOC)
47 dependent polynomial ECM was investigated for the electrochemical impedance spectroscopy of lithium-ion batteries (Q.
48 K. Wang, He, Shen, Hu, & Ma, 2018). The parameter identification method study of the Splice-Equivalent-Circuit-Model
49 (S-ECM) was realized for the aerial lithium-ion battery pack (S. L. Wang, Fernandez, Liu, Su, & Xie, 2018). A

50 Partnership-for-a-New-Generation-of-Vehicles (PNGV) modeling method together with the State-of-Charge (SOC)
51 prediction algorithm was studied for lithium-ion battery pack adopted in Automated Guided Vehicle (AGV) (Liu, Li, &
52 Zhou, 2018). A comparative study of different ECMs was investigated for the SOC estimation of lithium-ion batteries (Lai,
53 Zheng, & Sun, 2018) . Furthermore, another comparative study of reduced order ECMs was conducted for the on-board
54 state-of-available-power prediction of lithium-ion batteries (Farmann & Sauer, 2018).

55 The SOC prediction is very necessary for the group working lithium-ion batteries. And the dependent polynomial ECM
56 was realized for the electrochemical impedance spectroscopy of lithium-ion batteries (Q. K. Wang et al., 2018). The error
57 sources of the online SOC prediction methods were also investigated (Y. J. Zheng, Ouyang, Han, Lu, & Li, 2018). The
58 SOC inconsistency prediction was realized for lithium-ion battery packs by using the mean-difference model and
59 Extended-Kalman-Filter (EKF) algorithm (Y. J. Zheng, W. K. Gao, et al., 2018). Incremental capacity analysis and
60 differential voltage analysis based SOC and capacity prediction were conducted for lithium-ion batteries (L. F. Zheng, Zhu,
61 Lu, Wang, & He, 2018). An online SOC prediction algorithm was proposed for lithium-ion batteries by using an improved
62 adaptive cubature Kalman-Filter (KF) (Zeng, Tian, Li, & Tian, 2018). The SOC prediction was realized by using a novel
63 reduced order electrochemical model (Yuan, Wang, Zhang, Long, & Li, 2018). A double-scale and adaptive Particle-Filter
64 (PF) based online parameter identification method was investigated for the lithium-ion batteries (M. Ye, Guo, Xiong, & Yu,
65 2018). Furthermore, the online State-of-Health (SOH) prediction was implied for lithium-ion batteries by the Constant-
66 Voltage (CV) charging current analysis (J. F. Yang, Xia, Huang, Fu, & Mi, 2018). A novel Gaussian processed regression
67 model was investigated for the SOH prediction of lithium-ion battery by using the charging curve (D. Yang, Zhang, Pan,
68 Wang, & Chen, 2018).

69 Coupling SOC and SOH prediction effect was analyzed on the mechanical integrity of lithium-ion batteries (Xu et al.,
70 2018). Enhanced Coulomb counting method was conducted by using the Peukert Law and Columbic efficiency (Xie, Ma,
71 & Bai, 2018). Strong tracking effect of H-Infinity Filter was experimentally analyzed to realize the SOC prediction (Xia,
72 Zhang, et al., 2018). Online parameter identification and SOC prediction of lithium-ion batteries were investigated by using
73 the forgetting factor recursive least squares and the nonlinear KF algorithm (Xia, Lao, et al., 2018). Online model
74 identification and SOC estimation were realized for the lithium-ion battery with a recursive total least square based
75 observer method as stated by Wei *et al.* (Wei, Zou, Leng, Soong, & Tseng, 2018). De-noising wavelet treatment was

76 constructed for the SOC prediction of lithium-ion batteries (X. Wang, Xu, & Zhao, 2018) and an Unscented-Kalman-Filter
77 (UKF) observer was also designed for lithium-ion battery SOC prediction (T. P. Wang, Chen, Ren, & Zhao, 2018). An
78 adaptive SOC prediction method was proposed by us for an aeronautical lithium-ion battery pack based on a novel
79 Reduced-Particle-Unscented-Kalman-Filter (RP-UKF) (S. L. Wang, C. M. Yu, et al., 2018). In addition, an integrated
80 online adaptive SOC prediction approach was proposed by us for high-power lithium-ion battery packs (S. L. Wang,
81 Fernandez, Shang, Li, & Yuan, 2018). The improved SOC dependent polynomial ECM was constructed for
82 electrochemical impedance spectroscopy of lithium-ion batteries (Q. K. Wang et al., 2018) together with the influence
83 analysis of battery parametric uncertainties (Shoe et al., 2018).

84 By analyzing the online safety monitoring methods of lithium-ion battery packs in large and medium-sized UAVs, the
85 high-precision remaining available power prediction is realized, in which the effective State-of-Balance (SOB) evaluation
86 is investigated as well. Then, the safety monitoring equipment is developed for lithium-ion battery packs, laying the
87 foundation for the critical breakthroughs of the reliable power supply. The charge and discharge experiments are designed
88 and the nonlinear parameter identification experiments are also carried out, in which some working characteristics of the
89 lithium-ion battery packs can be obtained. Afterward, the S-ECM is introduced and the state-space equations are expressed
90 for the endurance prediction to improve its accuracy, which provides an experimental basis for the practical applications,
91 modeling simulation and battery management system design.

92 2. Mathematical analysis

93 Through the experimental analysis of lithium-ion battery packs used in the UAVs, the variation law of key factors can be
94 obtained and its rapid detection method is explored. The Voltage-Change-Rate (VCR) and the RP-UKF algorithms are
95 used to realize the online accurate SOC prediction. The variation coefficient calculation method is used to realize the
96 reliable SOB evaluation. In order to meet the reliable energy supply demand, the key technology research such as
97 parameter detection, online fault diagnosis, charging control and safety management, is carried out to realize the safety
98 monitoring equipment development. Technical application and promotion of the system anti-interference, charge and
99 discharge management and safety reliability enhancement are conducted. (1) The integrated chips and digital
100 communication methods are introduced to explore the application of high-precision, fast detection and anti-interference
101 processing technologies for the voltage, current and temperature parameters. (2) By using the application of the VCR and

102 the RP-UKF algorithm, the on-line high-accuracy SOC prediction is realized while reducing the hardware cost. (3)
103 Applying the variation coefficient calculation idea into the equilibrium state between the lithium-ion batteries of the pack
104 gives an accurate characteristic evaluation. In addition, its stable and reliable operation under complex conditions is
105 successfully achieved. (4) By Combining with the safety control and alarm, charge and discharge control, communication
106 and information storage requirement, a BMS equipment is developed for the UAV lithium-ion battery packs. It provides a
107 basis of the reliable power supply technology breakthrough.

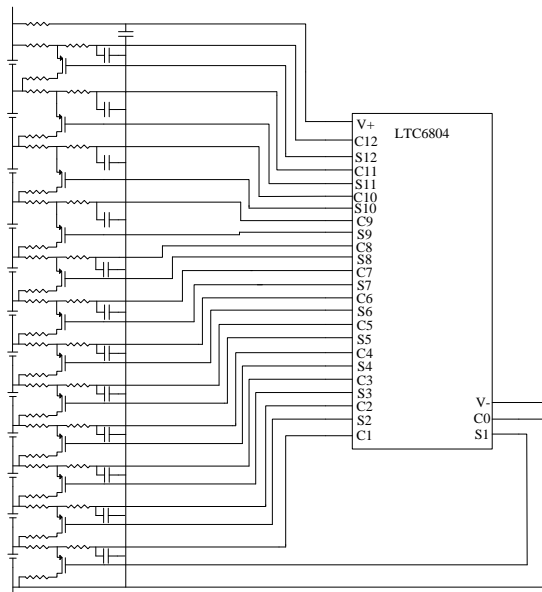
108 *2.1. Parameter detection and anti-interference*

109 Large and medium-sized UAVs have high requirements for the power supply of lithium-ion battery packs, the internal
110 structure of which has large number battery monomers in series and parallel combination characteristics. Aiming at its
111 high-precision and multi-channel signal detection requirements, the anti-jamming technology is researched and a high-
112 reliability detection scheme is designed to realize the multi-channel high-precision detection of key parameters such as
113 voltage, current and temperature for the lithium-ion battery packs. Considering the temperature gradient influence on the
114 detection accuracy, the signal detection and correction methods are studied, which are suitable for different ambient
115 temperatures. By analyzing the noise source of the signal detection process, the photoelectric isolation, transformer
116 isolation, grounding and other technical means are used to solve the anti-interference problem of power supply ripple,
117 electromagnetic interference and violent temperature changes.

118 During the operation of the lithium-ion battery packs, the detection of the external measurable parameter signal has an
119 inevitable error. At the same time, the noise introduced by the discrete digital sampling and iterative calculation processing
120 is difficult to eliminate, which leads to the cumulative error of the lithium-ion battery state prediction and the intelligent
121 management process. Considering the consistency influence over the monomers, once the equilibrium state information is
122 introduced into the lithium-ion battery ECM constructing process, how these characteristics can be reflected by using the
123 ECM needs to be solved. The expression of key time-varying parameter characteristics, such as voltage, current and
124 temperature, needs to be obtained through the experimental analysis. How to describe the correlation characteristics
125 between time-varying parameters in the battery pack of the perspective ECM requires in-depth studies. The proposed S-
126 ECM method can simulate the internal polarization effect, self-discharge and charge-discharge difference of the battery
127 packs, which is studied to realize the model characteristic expression of the grouped working lithium-ion batteries.

128 Furthermore, the state-space equation is constructed to reveal the variation law of external measurable parameters, which
129 lays a foundation to monitor the reliable energy state of lithium-ion battery packs.

130 Aiming for the large and medium-sized UAV application scenarios, the lithium-ion battery pack has a large number of
131 serials and parallel combination characteristics. In order to achieve the high-precision, multi-channel signal detection
132 targets, the anti-jamming technology and detection schemes are studied. Meanwhile, the key parameter detection of
133 lithium-ion battery is realized. Based on the high integrated chip and digital communication mechanism, the modular
134 design is conducted to realize the high-accuracy detection, the principle of which is shown in Fig. 1.



135

136

Fig. 1. key parameter detection sub-module

137 In order to solve the multi-channel and high-precision parameter detection problem of lithium-ion battery packs, the
138 influence of different parameters must be considered, such as: temperature gradient change of the detection accuracy, signal
139 detection as well as the correction method suitable for different temperature environments. The anti-interference problem of
140 power supply ripple, electromagnetic interference and other influencing factors should be solved, making it suitable for the
141 complex of UAV application scenarios. The following parameters should be analyzed: the signal detection noise source,
142 anti-interference ability, optical isolation, transformer isolation technologies.

143 2.2. Residual power prediction and construction

144 According to the new idea of calculating the SOC value according to the VCR, the SOC prediction model is constructed
145 together with the application of the proposed RP-UKF algorithm. And the recursive operation of the residual available

146 SOC value is realized for the lithium-ion battery packs. Combined with the battery working characteristic analysis of
147 complex working conditions, the improved S-ECM and its state-space equations are implied to improve the calculation
148 efficiency. The linearization process is optimized by streamlining the PF algorithm to eliminate the estimated offset and
149 utilize the equilibrium state. The feedback correction improves the prediction accuracy of the group working batteries, and
150 thus achieves the high-accuracy and online prediction of the remaining available power for the lithium-ion battery packs.

151 Lithium-ion battery grouping SOC prediction process is affected by the complex monomer structure and aging degree, as
152 well as environmental conditions such as the temperature and humidity. Therefore, the iterative calculation correction of
153 multiple factors needs to be considered in the SOC prediction process. By improving the iterative RP-UKF calculation
154 process, the prediction modelling implementation mechanism is explored, and a real-time optimization model is
155 constructed to provide an overall framework of the SOC prediction. Using high robust KF and its nonlinear extension,
156 combined with the Unscented Transformation (UT) and functional fitting approximation, the mathematical description of
157 working characteristics is explored for different working conditions. Through the modification of model parameters and
158 weighting factors, the influence of inter-monomer imbalance on the SOC prediction is analyzed, and an adaptive SOC
159 prediction model is constructed. Through the experiments, the action law of environmental conditions on the prediction
160 process can be obtained. The typical environmental simulation experiment is used to obtain the change law, and the
161 correction is made to optimize and correct the prediction results, which provides the theoretical basis of the improvement
162 on the SOC prediction adaptability under complex environmental conditions. The relationship between key parameters
163 such as voltage and temperature is obtained, and the influence law is analyzed experimentally. The iterative calculation,
164 correction and functional relationship optimization are used to improve the robustness effect of the SOC prediction model.

165 Through the reaction mechanism analysis and working condition simulation experiments, the internal reaction process of
166 the lithium-ion battery is clarified, and the variation rules of current, voltage and temperature are studied. The working
167 characteristics of different working conditions are obtained and established, together with the relationship between the
168 Closed Circuit Voltage (CCV), temperature and current. Combined with the working mode analysis under different
169 working conditions, the basic characteristic analyzing experiments are investigated for lithium-ion battery packs. Through
170 the experimental research of different magnification, cyclic charge and discharge, the key factors can be obtained. Based
171 on the simulation experiments at different working conditions, the output response and change trend of lithium-ion battery

172 pack under different working conditions can be obtained and analyzed. The working condition influence is discussed, and
173 the operating characteristic curves and variation laws of different working conditions are obtained. By using the battery
174 ECM and state-space equation expression, the mathematical description methods of different working conditions are
175 explored. Furthermore, using the high robust KF and its nonlinear extension algorithm, combined with the UT and function
176 fitting approximation, the adaptive remaining available power prediction model is constructed.

177 Based on the simulation and experimental analysis, the relationship between the remaining available electricity and SOB
178 between the monomers can be analyzed during the group working conditions. The model parameters and weighting factors
179 are modified to solve the influence of the imbalance between the monomers on the SOC prediction. On the basis of
180 simulation and experimental analysis, the influence of the equilibrium state is incorporated into the adaptive SOC
181 prediction process by using the mathematical SOB description. As a result, the model parameters and weighting factors are
182 corrected and the prediction model is improved. The remaining available power prediction is verified by the complex
183 working condition experiments, which is realized through the standard current charging, long-term shelving, intermittent
184 replenishment, rapid discharge and other experimental research. Through the normal state, over-charge and over-discharge
185 simulation conditions, the experimental verification of the remaining available power prediction is carried out under
186 complex conditions.

187 In order to improve the adaptability of the SOC prediction process, the voltage signal is used to detect the combined VCR
188 to achieve the accurate SOC prediction. In the implementation process, the intermediate parameters of U_A , SOB and
189 Rate_U are first calculated by using the mean monomer voltage value, variation coefficient and VCR. Afterwards, the
190 current value I_L under the influence of the complex working condition is obtained by using the functional calculation. The
191 obtained current parameter I_L and the equilibrium stated parameter SOB are used as input parameters, and the proposed S-
192 ECM model is constructed. Then, the corresponding state-space equation S_E can be obtained. Finally, the proposed real-
193 time SOC prediction is achieved by the proposed RP-UKF algorithm. In the SOC prediction process of the lithium-ion
194 battery pack, the real-time detected individual cell voltages of U_1, U_2, U_3, \dots and U_n are used as the main input parameters,
195 combined with the input of the temperature signal T . The RP-UKF algorithm is used for iterative calculation to obtain the
196 SOC value. The overall implementation structure block diagram is shown in Fig. 2.

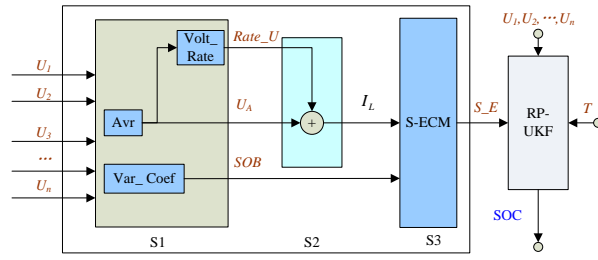


Fig. 2. SOC prediction structure

197

198

199 In the above figure, the overall structure of the lithium-ion battery state-space mathematical description is divided into
 200 three parts: S1, S2 and S3.

201 In the S1 section, the inlet parameters are the individual monomer voltages of U_1, U_2, U_3, \dots and U_n , and finally it is
 202 transformed into the state-space equation for the mathematical description. The module *Avr* is used to calculate the average
 203 voltage value U_A . The module *Volt_Rate* is used to obtain the VCR parameter *Rate_U*. And the module *Var_Coef* is used
 204 to find the inter-monomer balance state *SOB* as shown below.

205

$$U_A = \frac{1}{n}(U_1 + U_2 + U_3 + \dots + U_n) \quad (1)$$

206

$$Rate_U = h(U_{A1}, U_{A2}, U_{A3}, \dots, U_{Am}) \quad (2)$$

207

$$SOB = \theta^2 = \frac{1}{n} \sum_{i=1}^n \left(\frac{U_i - U_A}{U_A} \right)^2 \quad (3)$$

208 Wherein, n is the number of battery monomers in series, in which the parallel monomers used for expansion are taken as
 209 a single battery cell. U_1, U_2, U_3, \dots , and U_n are the respective monomer voltages. $U_{A1}, U_{A2}, U_{A3}, \dots$, and U_{Am} are the U_A
 210 values, which are obtained at the first m time moments in front of the present time. $h(*)$ is the functional relationship of the
 211 VCR. *SOB* is an equilibrium state between the internal connected battery monomers, which is obtained by calculating the
 212 square value of the variation coefficient θ . U_i is the voltage acquisition value of the i -th battery monomer at the present time.

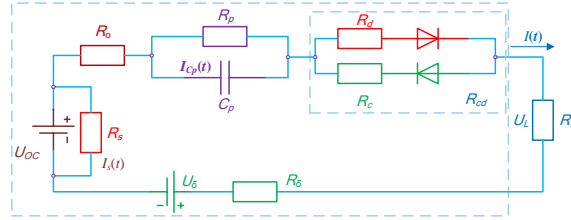
213 In the S2 plate, the mean voltage and change rate parameters are used to obtain the estimated operating current value I_L by
 214 the following functional relationship, which will replace the measured value to participate in the subsequent iterative
 215 calculations.

216

$$I_L = f(U_A, Rate_U) \quad (4)$$

217 In the S3 plate, the inlet parameter is the calculated current value I_L , and the balance state value *SOB*. In the real-time
 218 iterative calculation process, the proposed RP-UKF algorithm is adopted. The inlet parameters are the voltage signals of

219 each battery cells and the temperature, and the exit parameter is the SOC value of the group working lithium-ion batteries.
 220 The optimized real-time iterative calculation is used to obtain the accurate SOC value. The equivalent model S-ECM can
 221 be introduced as shown in **Error! Reference source not found.**

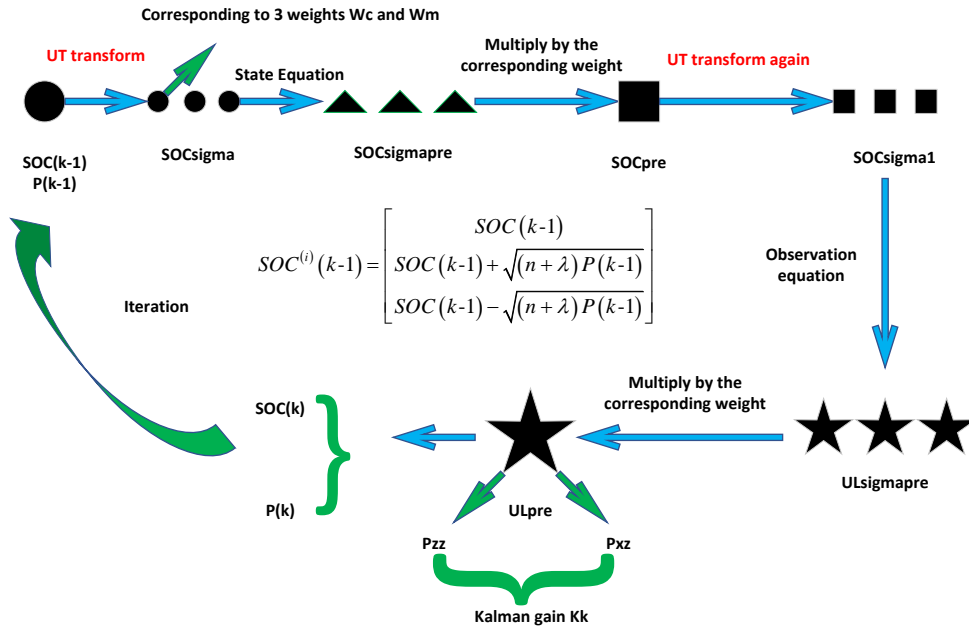


222
223 Fig. 3. S-ECM equivalent model

224 Through the Kirchhoff law and the SOC iterative calculation of mathematical expression of discrete time conditions, the
 225 state-space equation is obtained as shown in the Equation 5.

$$\begin{cases}
 SOC(k|k-1) = SOC(k-1) - \frac{\eta_r I(k) T_s}{Q_n} - \frac{I_s(k) * T_s}{Q_n} \\
 U_L(k) = (U_{oc} - U_\delta) - (R_o + R_s) * I(k) - I(k) R_p (1 - e^{-T_s / R_p C_p}) - I(k) R_{cd}
 \end{cases} \quad (5)$$

227 Based on the proposed RP-UKF algorithm, the simplified three-particle and double UT treatments are performed to
 228 improve the prediction accuracy and reduce the computational complexity. Furthermore, a specific implementation is
 229 performed for the real-time SOC prediction, the calculation flow of which is shown in Fig. 4.



230
231 Fig. 4. RP-UKF algorithm based SOC prediction flow

232 The above calculation makes full use of the voltage signal characteristics in the lithium-ion battery pack, and uses the
 233 characteristic information covered in the voltage signal obtained by the real-time detection instead of current signal changes
 234 to realize the effective real-time working state expression, reducing the hardware cost of the signal detection and the BMS
 235 volume. At the same time, the method can adapt to the SOC prediction of lithium-ion battery packs with different
 236 capacities by removing the dependence on the current signal detection, which greatly improves the adaptability of the
 237 algorithm. The ideal voltage source U_{OC} is used to indicate the OCV characteristics. U_L is the terminal voltage at both ends
 238 of the external load. The positive and negative of I_L characters the discharge and charge working conditions. The Ohm
 239 internal resistance R_o is determined by the internal structure of the battery and the electrolyte. The polarization internal
 240 resistance R_p is the resistance caused by the polarization effect when the positive and negative electrodes of the batteries are
 241 chemically reacted, and C_p is the polarization capacitance. The parallel circuit of R_p and C_p describes the polarization
 242 process. According to the working characteristics of the capacitor component, the relationship between the current flowing
 243 through the battery polarization capacitor and its CCV is shown in Equation 6.

$$244 \quad I_p(t) = C_p \frac{dU_{Cp}(t)}{dt} \quad (6)$$

245 It can describe the dynamic and static performance of lithium-ion batteries, which can simulate the battery behavior
 246 accurately under different current and temperature conditions in the charge and discharge process. Its structure is relatively
 247 simple and has been widely used in the dynamic modeling of power batteries. When the battery is charged and discharged,
 248 the accumulation of current in time causes a SOC change. R_o represents the ohm internal resistance. I_L is its load current,
 249 and U_L is the terminal voltage. These parameters need to be obtained by HPPC experiments.

250 The applied mathematical modelling approach is compared with other approaches that are used in the working state
 251 estimation and prediction process of the lithium-ion batteries. The main features and innovations of this method compared
 252 with other approaches are as follows: (1) A composite equivalent circuit modeling method is proposed to accurately
 253 describe the working characteristics. (2) Based on the improved UKF algorithm, a new model of group working state
 254 prediction is constructed. (3) Explanatorily apply key factors such as equilibrium state are introduced to the correction
 255 process of SOC prediction. Through the simulation of the dynamic auxiliary power simulation and the prediction effect
 256 analysis, the effective characterization of the remaining power of the power lithium battery pack is realized, in which the
 257 computational complexity is reduced and the prediction accuracy is improved.

258 2.3. *Reliable equilibrium state evaluation*

259 The equilibrium state is introduced into the ECM modeling analysis process during the SOC prediction process of the
260 group working lithium-ion batteries. Furthermore, these characteristics should to be reflected off the ECM, and applied to
261 the iterative calculation processes of the SOC prediction for the battery packs. Based on the mathematical description of the
262 monomer voltage difference, the equilibrium stated modeling and the correction methods are developed to describe the
263 inconsistent state between the monomers. Furthermore, the model parameters are combined with the weighting factors,
264 which are embedded in the iterative SOC calculation processes. And the iterative calculation process is implemented with
265 modularity to eliminate the monomer difference influence on the SOC prediction accuracy of the group working lithium-
266 ion batteries. Through the modification of model parameters and weighting factors, it can make a reliable numerical
267 evaluation of the equilibrium state between the lithium-ion battery monomers. Using the monomer voltage to achieve the
268 inter-monomer SOB evaluation, a novel numerical description can be conducted. Combined with the variation coefficient
269 calculation in statistics, the equilibrium stated characteristic between the monomers of the power lithium-ion battery pack is
270 expressed. Finally, the effect of inter-body consistency difference is described in the correction section to eliminate the
271 impact on the inter-monomer inconsistency of the SOC prediction.

272 The lithium-ion battery packs utilize complex cascade structures to break the limitations of low voltage and small
273 capacity of the battery monomers. Due to the inevitable monomer difference in the manufacturing and application process,
274 the imbalance between the internal monomers of the battery pack occurs, which causes safety hazards in the practical
275 applications and affects the accuracy of the group working SOC prediction. Therefore, it is necessary to study the
276 evaluation method of the equilibrium state and apply it to the correction step of the prediction process. During the
277 application of lithium-ion battery packs, the difference between monomers will increase along with time. Based on the
278 calculation of the variation coefficient, the evaluation and characterization of the equilibrium state are realized. The
279 implementation idea is shown in Fig. 5.

Avr:

$$E(U_c) = \bar{U}_c = \frac{1}{n} \sum_{i=1}^n U_{ci}$$

Var:

$$\delta^2 = \frac{1}{n} \sum_{i=1}^n (U_{ci} - E(U_c))^2$$

Coe_Var:

$$\theta = \frac{\delta}{E(U_c)} = \sqrt{\frac{1}{n} \sum_{i=1}^n \left(\frac{U_{ci} - E(U_c)}{E(U_c)} \right)^2}$$

Squ_Var:

$$SOB = \varepsilon = \theta^2 = \frac{1}{n} \sum_{i=1}^n \left(\frac{U_{ci} - E(U_c)}{E(U_c)} \right)^2$$

$$\begin{cases} U_\delta(k) = \varepsilon * U_{oc}(k) = \frac{1}{n} \sum_{i=1}^n \left(\frac{U_{ci}(k) - E(U_c(k))}{E(U_c(k))} \right)^2 * U_{oc}(k) \\ R_\delta(k) = \varepsilon * R_o(k) = \frac{1}{n} \sum_{i=1}^n \left(\frac{U_{ci}(k) - E(U_c(k))}{E(U_c(k))} \right)^2 * R_o(k) \end{cases}$$

Evaluate the equilibrium state

280

281

Fig. 5. State of balance evaluation

282

283

284

285

286

287

288

2.4. Battery management equipment development

289

290

291

292

293

294

295

The development of supporting safety monitoring equipment for lithium-ion battery packs embedded in large and medium-sized UAV is mainly realized through the state parameter detection, online fault diagnosis, charging control, safety control and alarm, communication and information storage. Furthermore, the thermal runaway control strategy is studied together with security monitoring and alarm by using the intelligent management strategy and implementation technologies. When the fault is diagnosed, the controller is notified and the processing request is sent to command. When the threshold value is exceeded, the main loop power is cut off to prevent high temperature and over-discharge phenomenon. The system structure of BMS is shown in Fig. 6.

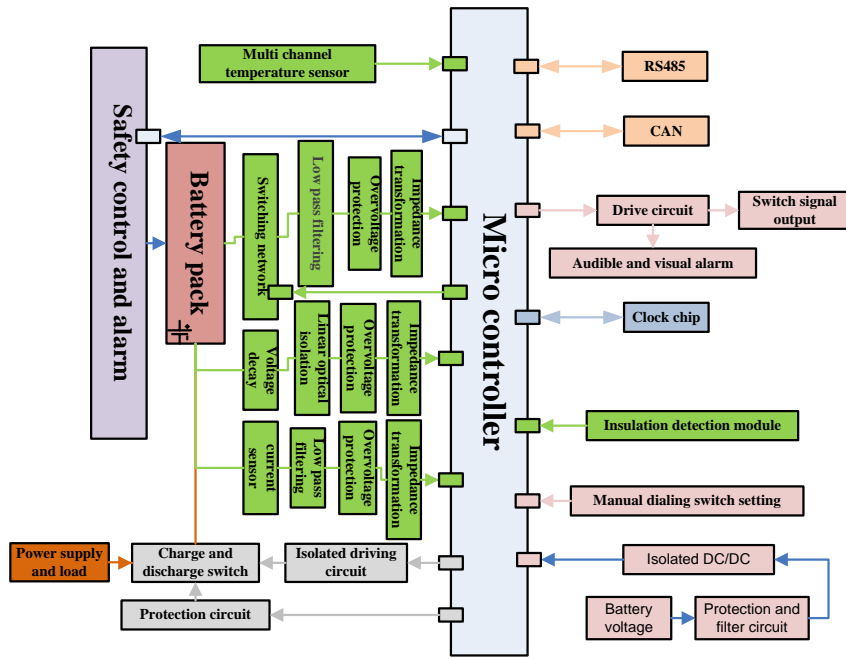


Fig. 6. Supporting safety monitoring equipment structure

296

297

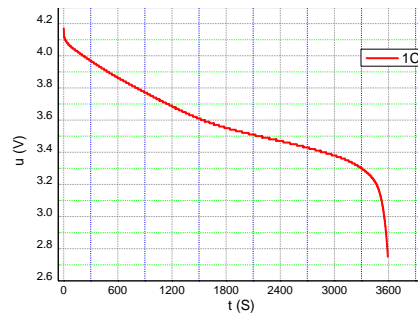
298 As can be seen from the above Figure, the safety monitoring technologies of lithium-ion battery packs are studied for the
 299 large and medium-sized UAVs. In addition, the remaining available power prediction model is embedded in the BMS to
 300 realize the online accurate SOC prediction. The key technology research is conducted, such as parameter detection, online
 301 fault diagnosis, battery safety control and alarm, charging control. And then, the development of supporting safety
 302 monitoring equipment is realized to ensure the safe and reliable operation of lithium-ion battery packs. The power lithium-
 303 ion battery pack is maintained at a good operating temperature by using a heater chip and a heat sink. Based on the
 304 functional and performance requirements of the power application, a working state detection and analysis subsystem is
 305 designed. The operational status detection and analysis includes the SOC prediction of the power lithium battery pack to
 306 ensure its safe application for its energy storage and energy supply processes. The data transmission uses the digital signals
 307 with strong anti-interference ability, and realizes real-time voltage, current and temperature signal detection during charging
 308 and discharging process. Compared with other systems, the improved equivalent model building and endurance prediction
 309 methods are introduced in our scientific research, which is put forward considering the characterization accuracy and
 310 computational complexity by using the improved equivalent circuit modeling method together with the RP-UKF algorithm
 311 investigation. The comprehensive SOB evaluation is conducted real-timely for the internal connected battery cells, which is
 312 implied into the iterative calculation process. The corresponding anti-interference processing is carried out and the

313 correction algorithm is employed for the obtained function relation when it is applied to the on-line state prediction process
314 of the safety control system for the lithium-ion battery packs.

315 3. Experimental analysis

316 3.1. Charging and discharging process

317 In order to get the basic working characteristics of the lithium-ion battery packs used in the UAVs, this experiment
318 monitors the electricity variation in real-time. The lithium cobaltate (LiCoO₂) battery pack is selected as the experimental
319 sample, which consists of M cells connected in series, heating components, sampling resistors, temperature sensors, sockets
320 and combined cover. Combined with the application of temperature sensors, cross-type connectors and electronic
321 connectors, the organic combination of multiple components is realized. The proposed method is applicable to different
322 types of lithium-ion battery packs, and only needs to modify the coefficient values of the functional relationships, which
323 will be obtained by parameter identification. The voltage and current changes are analyzed for the working state monitoring
324 under different working conditions, and the voltage variation law can be obtained towards time. The relationship is shown
325 in Fig. 7.



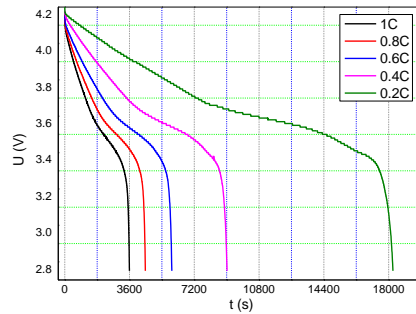
326

327

Fig. 7. Charge and discharge characteristics

328 Firstly, 1C Constant-Current (CC) charging treatment is used for the fast charging process of the charging phase. The
329 voltage has a fast rising phase, a slow rising phase, and a fast rising phase again. When the voltage rises to the rated
330 terminal charging voltage, the current decreases gradually until the current drops to 0.05C when the charging is at the end
331 by using the CC-CV charging treatment. Then, the lithium-ion battery pack is left for 1 hour to make the internal reaction
332 returns to the steady state. The discharge test is conducted by 1C CC discharging. When the voltage drops to the end
333 discharge voltage, the discharge process is the end. In the discharge process, the whole figure can be divided into three
334 parts, which are: the voltage of the first part in the CC discharge process is rapidly decreased. The voltage dropped rate of

335 the second part decreases slowly, and the voltage dropped speed of the third part is fast. The discharge is terminated by the
336 drop to the discharge termination voltage. The different charge and discharge curves obtained by controlling the current
337 magnifications of 0.5C, 1C and 1.5C are shown in Fig. 8.

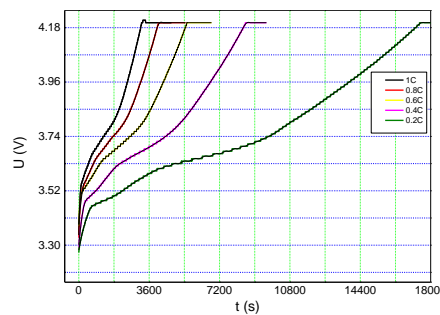


338

339

Fig. 8. Discharge at different rates

340 During the discharge process of the lithium-ion battery, most of the time is in the second part, and the length of time
341 occupied by the second part reflects the health state and the battery working performance. The multiple charging
342 characteristics are shown in Fig. 9.

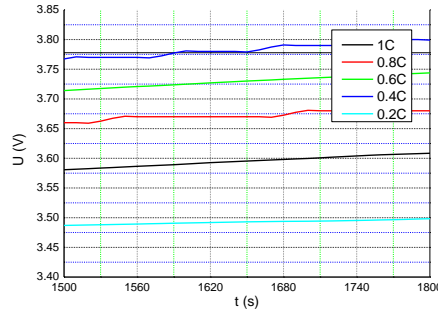


343

344

Fig. 9. Charge at different rates

345 This is the voltage variation curve under different charge and discharge current rate conditions. Its variation law is studied,
346 and a new method is explored for the SOC prediction. At present, the difference seen by the naked eye is quite large and
347 the difference is obvious, but this is seen under the premise of large compression in the time axis. In a short time-frame, the
348 change will be very insignificant. In order to obtain the voltage change rate law, the charge curve is amplified locally. The
349 functional change law is observed and obtained as shown in Fig. 10.



350

351

Fig. 10. Local charge at different rates

352

353

354

355

The voltages are the same and the slopes are different. According to the one-to-one correspondence between the different slopes and the discharge current, the discharge current can be obtained. Afterward, only voltages need to be measured to get the current, which is then used estimate the SOC value.

3.2. OCV-SOC nonlinear parameter identification

356

357

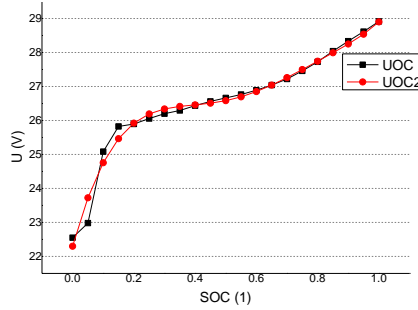
358

359

360

361

At the room temperature of 25°C, the lithium-ion battery was filled and allowed to stand for 1 hour by the CC-CV charging method, and the internal reaction was returned to a stable state. The CC discharge was performed at a discharge rate of 1 C. When the 10% SOC is released, it is set to stand for 30 minutes. The cyclic operation is performed for 10 times, and the voltage versus time curve is obtained. OCV is the terminal voltage of the battery in the open state, which can be recorded after standing for 30 minutes for every 10% SOC release in the experiment. And the OCV-SOC relationship curve at 1C discharging rate is obtained as shown in Fig. 11.



362

363

Fig. 11. OCV-SOC curve at 1C discharge rate

364

The curve fitting result of the OCV-SOC relationship is shown in Equation 7.

365

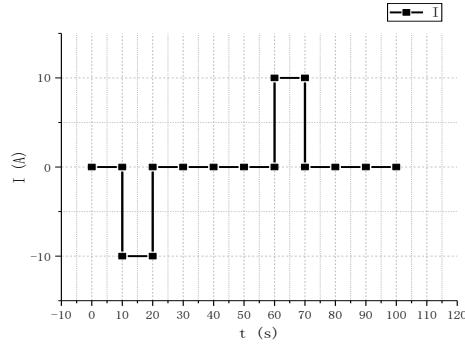
$$U_{oc} = f(\varphi) = a_0 + a_1\varphi + a_2\varphi^2 + a_3\varphi^3 + a_4\varphi^4 + a_5\varphi^5 + a_6\varphi^6 \quad (7)$$

366

Wherein, $a_0=22.3$, $a_1=32.9$, $a_2=-92.4$, $a_3=86.6$, $a_4=50.9$, $a_5=-125.3$, $a_6=53.9$.

367 3.3. Pulse power experimental test

368 The Hybrid Pulse Power Characterization (HPPC) tests are very important, which are used commonly in the parameter
369 identification process. It is currently used by mounts of battery manufacture and UAV companies to evaluate the
370 performance of the battery systems and modules. A single HPPC test is shown in Fig. 12.



371

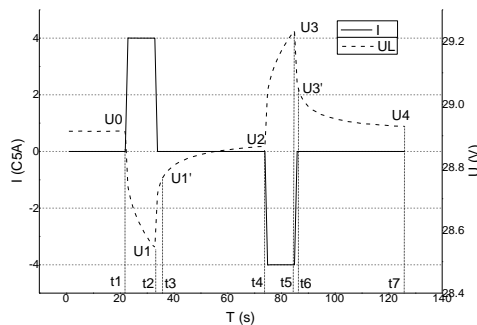
372

Fig. 12. HPPC test current curve

373 In the first step, the lithium-ion battery is subjected to a 1C rate CC pulse discharge 10 seconds, which will be set aside for
374 40 seconds in the second step. In the third step, the lithium-ion battery is charged with a CC pulse of 10C at a rate of 10C.
375 In the cycle test, the lithium-ion battery is fully charged by CC-CV charging, and the SOC value is reduced to 90%, 80%,
376 ..., 10% by CC discharging for 40 minutes. The HPPC test is performed under the SOC value, and the voltage change
377 relationship to time can be obtained.

378 3.4. Model parameter identification

379 The test was carried out at a temperature of 25°C to identify the parameters in the ECM, such as the ohm internal
380 resistance R_o , the polarization internal resistance R_p and the polarization capacitance C_p . Taking the SOC of 0.95 as an
381 example, the single cycle HPPC tested voltage response curve is obtained as shown in Fig. 13.



382

383

Fig. 13. HPPC single test curve

384 (1) The parameter identification of ohm internal resistance R_o is conducted by using the following treatment. The current
 385 changes at time t_1 , and the sudden changes of voltage U_0 to U_1 are caused by the ohm internal resistance R_o , so its value can
 386 be obtained by Equation 8.

$$387 \quad R_o = \frac{\Delta U}{I} = \frac{U_0 - U_1}{I} \quad (8)$$

388 (2) Parameter identification of polarization internal resistance R_p can be investigated as follows. During the static stage of
 389 t_3 - t_4 , the polarization capacitance C_p is discharged through R_p , and the voltage is slowly increased to U_2 by U_1' . The
 390 magnitude of the rise is determined by R_p , so its value can be obtained by using Equation 9. Wherein, I is the discharge
 391 current.

$$392 \quad R_p = \frac{\Delta U'}{I} = \frac{U_2 - U_1'}{I} \quad (9)$$

393 (3) Parameter identification of time constant can be investigated as follows. The same analysis of the t_3 - t_4 static stage, the
 394 zero input response to the parallel RC circuit of this stage can be implied to obtain the OCV value by using Equation 10.

$$395 \quad U_{oc} = U_1 - U_{cp} = U_1(1 - e^{-\frac{t}{\tau}}) \quad (10)$$

396 As can be known from the above Equation, U_1' and U_2 can be obtained as shown in Equation 11 and 12.

$$397 \quad U_1' = U_0(1 - e^{-\frac{t_3}{\tau}}) \quad (11)$$

$$398 \quad U_2 = U_0(1 - e^{-\frac{t_4}{\tau}}) \quad (12)$$

399 Furthermore, the time constant of the simultaneous Equations can be obtained as shown in Equation 13.

$$400 \quad \tau = -\frac{t_4 - t_3}{\ln\left(\frac{U_0 - U_2}{U_0 - U_1'}\right)} \quad (13)$$

401 (4) Parameter identification of the polarization capacitor C_p can be obtained, after obtaining R_p , which is shown in
 402 Equation 14.

$$403 \quad C_p = \frac{\tau}{R_p} \quad (14)$$

404 According to the HPPC test data, the values of various parameters are calculated, as shown in Table 1.

405 Tab.1 The parameter value of HPPC test and calculation

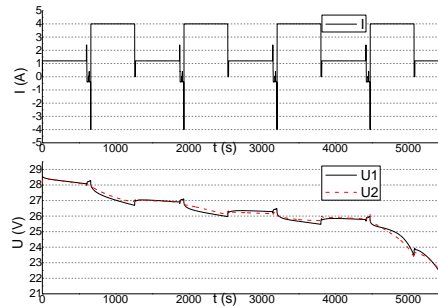
| SOC | R_o / m Ω | R_p / m Ω | C_p /F | U_{oc} /V |
|-----|--------------------|--------------------|----------|-------------|
| 1 | 20.7 | 1.49 | 93317.1 | 3.4 |

| | | | | |
|-----|-------|------|---------|-------|
| 0.9 | 18.6 | 1.16 | 49748.1 | 3.34 |
| 0.8 | 15.7 | 1.06 | 54440.5 | 3.32 |
| 0.7 | 17.9 | 1.02 | 56575.4 | 3.3 |
| 0.6 | 17.1 | 1.36 | 42431.6 | 3.296 |
| 0.5 | 19.55 | 1.21 | 47691.7 | 3.294 |
| 0.4 | 20.3 | 1.59 | 36294.2 | 3.29 |
| 0.3 | 23.4 | 1.67 | 34555.5 | 3.27 |
| 0.2 | 24.9 | 1.46 | 39525.8 | 3.25 |
| 0.1 | 28.6 | 1.59 | 22899.1 | 3.21 |

406 As can be known from the experimental data analysis, the mean value of ohm internal resistance R_o is 20.68 m Ω . The
407 mean value of the polarization internal resistance R_p is 1.36 m Ω , and the mean value of polarization capacitance C_p is
408 24421.7F. The ohm internal resistance R_o does not change significantly into the discharge process. As the SOC value
409 decreases, there is a slightly rising process. The polarization internal resistance R_p has little change along with the SOC
410 value, and there is no obvious rising or falling trend. Therefore, the average values are selected as the polarization internal
411 resistance values. The polarization capacitance C_p decreases along with the SOC value, and it increases gradually.

412 3.5. The SOC prediction effect

413 The M-ICPXX power lithium-ion battery pack was selected as the experimental sample, which was mainly composed of
414 medium-sized ICPXX lithium-ion battery cells, heating components, sampling resistors, temperature sensors, sockets and
415 composite cover. The combination, combined with the application of temperature sensors, cross-connectors and electrical
416 connectors, enables the organic combination of multiple components. The string XX represents the rated capacity of the
417 lithium-ion battery pack. The single cells are composed of a plurality of batteries connected with parallel and confluent,
418 which is sealed by a battery cell shell and a single cell cover. The heating component includes a polyimide heating film and
419 a heating frame. During the application process of the lithium-ion battery pack, the battery cells formed by the respective
420 parallel battery cells need to be cascaded in series to meet the high voltage and large capacity requirements of the UAV
421 power application. According to the power demand, the number of commonly used series lithium-ion monomers should be
422 6, 7, and 14. In the experimental analysis process, the lithium-ion battery pack and its internal connected monomers were
423 selected for the experimental analysis.



424

425

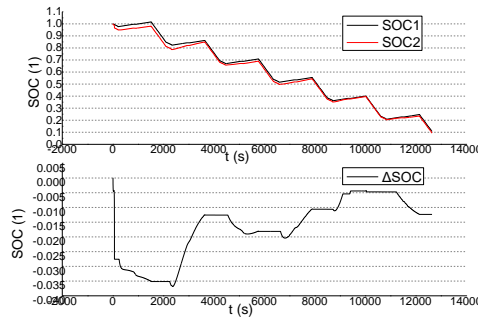
Fig. 14. CCV tracking effect

426

As can be known from the experimental data, the effective CCV tracking and the SOC estimation can be realized under

427

complex working conditions.



428

429

Fig. 15. SOC prediction effect

430

After comparison of the results obtained by the Ah-based integral method, the error between the iterative calculated value

431

and the ampere-hour integral value is stable within 2.00%. It can be seen from the experimental data shown in the figure

432

that the tracking error of the CCV in the complex working condition is 1.00%, and the error between the iterative

433

calculation value and the ampere-hour integral value is stable within 2.00%. Experimental data shows that this method can

434

achieve the effective CCV tracking and SOC prediction.

435 4. Conclusions

436 The endurance prediction of the power lithium battery pack plays an important role in its energy and safety management,

437 which is an important part of the clean production and the reasonable battery energy management will facilitating its

438 smooth implementation. A new endurance capability predicting method is proposed and realized, which improves the

439 prediction accuracy and reduces the iterative computational complexity. The experimental verification is conducted,

440 combining with the theoretical analysis, model construction, equipment development and experimental verification. In

441 view of the reliable energy management and safety control objectives of lithium-ion battery pack, the battery equivalent

442 modeling construction method is explored and the adaptive residual available power prediction along with equilibrium state
443 evaluation is realized. In combination with the application scenario analysis of large and medium-sized UAVs, a safety
444 monitoring equipment is developed to conduct the reliable energy management and safety controls. And weighed the
445 complexity and accuracy, the improved ECM has been constructed by using the HPPC test of the parameter identification.
446 The charge and discharge experiments and nonlinear curve identification experiments are carried out to analyze the partial
447 operating characteristics of the lithium-ion batteries, which are also used to verify the prediction effect. It provides
448 experimental basis of the future practical applications, modeling simulation and BMS design. In the future, the following
449 aspects will be further studied: (1) The equivalent modeling methods of group working characteristics by using the
450 electronic components. (2) The calculation improvement on the unscented transformation weights and the Kalman
451 superposition correction factor. (3) The expansion and correction strategy of the influence parameters.

452 **Acknowledgments**

453 This research was supported by National Natural Science Foundation (No. 61801407), Sichuan Province Science and
454 Technology Support Program (No. 2018GZ0390, 2017FZ0013), Scientific Research Fund of Sichuan (No. 17ZB0453),
455 Sichuan Science and Technology Innovation Miao-Zi Project (No. 2017109), Teaching Research Project (18gjzx11,
456 18dsts16), Sichuan Science and Technology Innovation Cultivation Project (No. 201710619112). In addition, CF would
457 like to express his gratitude to RGU for its support. Thanks to the sponsors.

458 **References**

- 459 Carkhuff, B. G., Demirev, P. A., & Srinivasan, R. (2018). Impedance-Based Battery Management System for
460 Safety Monitoring of Lithium-ion Batteries. *Ieee Transactions on Industrial Electronics*, 65(8), 6497-
461 6504.
- 462 Farmann, A., & Sauer, D. U. (2018). Comparative study of reduced order equivalent circuit models for on-board
463 state-of-available-power prediction of lithium-ion batteries in electric vehicles. *Applied Energy*, 225,
464 1102-1122.

465 Hannan, M. A., Hoque, M. M., Hussain, A., Yusof, Y., & Ker, P. J. (2018). State-of-the-Art and Energy
466 Management System of Lithium-ion Batteries in Electric Vehicle Applications: Issues and
467 Recommendations. *Ieee Access*, 6, 19362-19378.

468 He, F. Q., Li, X. X., Zhang, G. Q., Zhong, G. J., & He, J. S. (2018). Experimental investigation of thermal
469 management system for lithium-ion batteries module with coupling effect by heat sheets and phase
470 change materials. *International Journal of Energy Research*, 42(10), 3279-3288.

471 Lai, X., Zheng, Y. J., & Sun, T. (2018). A comparative study of different equivalent circuit models for estimating
472 SOC of lithium-ion batteries. *Electrochimica Acta*, 259, 566-577.

473 Li, K., Yan, J. J., Chen, H. D., & Wang, Q. S. (2018). Water cooling based strategy for lithium-ion battery pack
474 dynamic cycling for thermal management system. *Applied Thermal Engineering*, 132, 575-585.

475 Liu, X. Y., Li, W. L., & Zhou, A. G. (2018). PNGV Equivalent Circuit Model and SOC Prediction Algorithm for
476 Lithium-ion Battery Pack Adopted in AGV Vehicle. *Ieee Access*, 6, 23639-23647.

477 Mathew, M., Janhunen, S., Rashid, M., Long, F., & Fowler, M. (2018). Comparative Analysis of Lithium-ion
478 Battery Resistance Prediction Techniques for Battery Management Systems. *Energies*, 11(6).

479 Mondal, B., Lopez, C. F., Verma, A., & Mukherjee, P. P. (2018). Vortex generators for active thermal
480 management in lithium-ion battery systems. *International Journal of Heat and Mass Transfer*, 124,
481 800-815.

482 Omariba, Z. B., Zhang, L. J., & Sun, D. B. (2018). Review on Health Management System for Lithium-ion
483 Batteries of Electric Vehicles. *Electronics*, 7(5).

484 Saw, L. H., Poon, H. M., Thiam, H. S., Cai, Z. S., Chong, W. T., Pambudi, N. A., & King, Y. J. (2018). Novel thermal
485 management system using mist cooling for lithium-ion battery packs. *Applied Energy*, 223, 146-158.

486 Shoe, A. I., Meng, J. H., Shoe, D. I., Swierczynski, M., Teodorescu, R., & Kaer, S. K. (2018). Influence of Battery
487 Parametric Uncertainties on the SOC Prediction of Lithium-ion Titanate Oxide-Based Batteries.
488 *Energies*, 11(4).

- 489 Wang, Q. K., He, Y. J., Shen, J. N., Hu, X. S., & Ma, Z. F. (2018). SOC-Dependent Polynomial Equivalent Circuit
490 Modeling for Electrochemical Impedance Spectroscopy of Lithium-ion Batteries. *Ieee Transactions on*
491 *Power Electronics*, 33(10), 8449-8460.
- 492 Wang, S. L., Fernandez, C., Liu, X. H., Su, J., & Xie, Y. X. (2018). The parameter identification method study of
493 the splice equivalent circuit model for the aerial lithium-ion battery pack. *Measurement & Control*,
494 51(5-6), 125-137.
- 495 Wang, S. L., Fernandez, C., Shang, L. P., Li, Z. F., & Yuan, H. F. (2018). An integrated online adaptive SOC
496 prediction approach of high-power lithium-ion battery packs. *Transactions of the Institute of*
497 *Measurement and Control*, 40(6), 1892-1910.
- 498 Wang, S. L., Yu, C. M., Fernandez, C., Chen, M. J., Li, G. L., & Liu, X. H. (2018). Adaptive SOC Prediction Method
499 for an Aeronautical Lithium-ion Battery Pack Based on a Reduced Particle-unscented Kalman Filter.
500 *Journal of Power Electronics*, 18(4), 1127-1139.
- 501 Wang, T. P., Chen, S. Z., Ren, H. B., & Zhao, Y. Z. (2018). Model-based unscented Kalman filter observer design
502 for lithium-ion battery state of charge prediction. *International Journal of Energy Research*, 42(4),
503 1603-1614.
- 504 Wang, X., Xu, J., & Zhao, Y. F. (2018). Wavelet Based Denoising for the Prediction of the State of Charge for
505 Lithium-ion Batteries. *Energies*, 11(5).
- 506 Wang, X. M., Xie, Y. Q., Day, R., Wu, H. W., Hu, Z. L., Zhu, J. Q., & Wen, D. S. (2018). Performance analysis of a
507 novel thermal management system with composite phase change material for a lithium-ion battery
508 pack. *Energy*, 156, 154-168.
- 509 Wei, Z. B., Zou, C. F., Leng, F., Soong, B. H., & Tseng, K. J. (2018). Online Model Identification and SOC Estimate
510 for Lithium-ion Battery With a Recursive Total Least Squares-Based Observer. *Ieee Transactions on*
511 *Industrial Electronics*, 65(2), 1336-1346.
- 512 Won, I. K., Choo, K. M., Lee, S. R., Lee, J. H., & Won, C. Y. (2018). Lifetime Management Method of Lithium-ion
513 battery for Energy Storage System. *Journal of Electrical Engineering & Technology*, 13(3), 1173-1184.

514 Xia, B. Z., Lao, Z. Z., Zhang, R. F., Tian, Y., Chen, G. H., Sun, Z., . . . Wang, H. W. (2018). Online Parameter
515 Identification and State of Charge Prediction of Lithium-ion Batteries Based on Forgetting Factor
516 Recursive Least Squares and Nonlinear Kalman Filter. *Energies*, 11(1).

517 Xia, B. Z., Zhang, Z., Lao, Z. Z., Wang, W., Sun, W., Lai, Y. Z., & Wang, M. W. (2018). Strong Tracking of a H-
518 Infinity Filter in Lithium-ion Battery State of Charge Prediction. *Energies*, 11(6).

519 Xie, J. L., Ma, J. C., & Bai, K. (2018). Enhanced Coulomb Counting Method for SOC Prediction of Lithium-ion
520 Batteries based on Peukert's Law and Coulombic Efficiency. *Journal of Power Electronics*, 18(3), 910-
521 922.

522 Xu, J., Jia, Y., Liu, B., Zhao, H., Yu, H., Li, J., & Yin, S. (2018). Coupling Effect of State-of-Health and SOC on the
523 Mechanical Integrity of Lithium-ion Batteries. *Experimental Mechanics*, 58(4), 633-643.

524 Yang, D., Zhang, X., Pan, R., Wang, Y. J., & Chen, Z. H. (2018). A novel Gaussian process regression model for
525 state-of-health prediction of lithium-ion battery using charging curve. *Journal of Power Sources*, 384,
526 387-395.

527 Yang, J. F., Xia, B., Huang, W. X., Fu, Y. H., & Mi, C. (2018). Online state-of-health prediction for lithium-ion
528 batteries using constant-voltage charging current analysis. *Applied Energy*, 212, 1589-1600.

529 Ye, M., Guo, H., Xiong, R., & Yu, Q. Q. (2018). A double-scale and adaptive particle filter-based online
530 parameter and state of charge prediction method for lithium-ion batteries. *Energy*, 144, 789-799.

531 Ye, X., Zhao, Y. H., & Quan, Z. H. (2018). Thermal management system of lithium-ion battery module based on
532 micro heat pipe array. *International Journal of Energy Research*, 42(2), 648-655.

533 Yuan, C. C., Wang, B. J., Zhang, H. Z., Long, C., & Li, H. H. (2018). SOC Prediction of Lithium-ion Battery Based on
534 a Novel Reduced Order Electrochemical Model. *International Journal of Electrochemical Science*, 13(1),
535 1131-1146.

536 Zeng, Z. B., Tian, J. D., Li, D., & Tian, Y. (2018). An Online State of Charge Prediction Algorithm for Lithium-ion
537 Batteries Using an Improved Adaptive Cubature Kalman Filter. *Energies*, 11(1).

538 Zheng, L. F., Zhu, J. G., Lu, D. D. C., Wang, G. X., & He, T. T. (2018). Incremental capacity analysis and
539 differential voltage analysis based state of charge and capacity prediction for lithium-ion batteries.
540 *Energy, 150*, 759-769.

541 Zheng, Y. J., Gao, W. K., Ouyang, M. G., Lu, L. G., Zhou, L., & Han, X. B. (2018). SOC inconsistency prediction of
542 lithium-ion battery pack using mean-difference model and extended Kalman filter. *Journal of Power*
543 *Sources, 383*, 50-58.

544 Zheng, Y. J., Ouyang, M. G., Han, X. B., Lu, L. G., & Li, J. Q. (2018). Investigating the error sources of the online
545 state of charge prediction methods for lithium-ion batteries in electric vehicles. *Journal of Power*
546 *Sources, 377*, 161-188.

547